An analytical model for the flow of collisionless plasma along magnetic fields

Justin M. Little* and Edgar Y. Choueiri†

Electric Propulsion and Plasma Dynamics Laboratory, Princeton University, Princeton, NJ, 08544

An analytical model is derived to study the two-dimensional character of axisymmetric, collisionless plasma flow along a guiding magnetic field. This is accomplished using a transformation from cylindrical to magnetic coordinates, which enables the separate treatment of the flow-averaged plasma parameters from their spatial non-uniformities. The result gives analytical solutions for the spatial variation of the potential, plasma density, and ion Mach number. Application of the model to the problem of supersonic plasma expansion from a magnetic nozzle shows good agreement with both numerical simulations and experimental measurements. Notably, the development of a downstream radial electric field to preserve quasi-neutrality is the main factor that drives non-uniformities within the plasma. This result is used to explain experimentally observed focusing of the plasma exhaust with respect to the applied magnetic field. Finally, the competition in the expansion process, between the conversion of thermal energy into kinetic energy and the loss to plume divergence of the kinetic energy useful for propulsion yields an expression for the maximum thrust coefficient of a magnetic nozzle in terms of the parameters of the plasma source.

I. Introduction

The application of simplified analytical models to describe plasma flowing through a cylindrically symmetric magnetic nozzle has been used to develop an understanding of ion acceleration and momentum transfer in such flows. The inclusion of two-dimensional effects to study spatial non-uniformities in the flow, however, has not been rigorously attempted. This is despite numerical and experimental evidence indicating the importance of spatial non-uniformities on phenomena such as exhaust focusing, plasma current generation, and quasi-neutrality. In addition to its fundamental value, a two-dimensional analytical model could aid plasma detachment investigations and improve fully analytical thrust and efficiency models.

In its idealized limit, plasma flow through a magnetic nozzle exhibits many similarities to gas flow through a conventional de Laval nozzle. The dominant physical process is the conversion of thermal energy into kinetic energy. The exhaust velocity of the plasma ions scales as the square of the ratio of the plasma temperature to the ion mass. A sonic conditions exists at the nozzle "throat," or point of minimal cross-sectional flow area, where the ion velocity is equal to the local ion-acoustic velocity. Furthermore, the force balance between the thermally expanding plasma and applied magnetic field induces azimuthal currents that transfer momentum to the source of the applied field: a phenomenon which parallels the transfer of momentum by the pressure distribution to the solid walls of a de Laval nozzle.

Given these similarities, it is no surprise that the quasi one-dimensional compressible flow equations, classic to conventional rocket nozzle design,[1] have been oftentimes found appropriate to describe the general behavior of plasma flow in magnetic nozzles. The ability of this simple analytical framework to describe the sub-to-super sonic transition was first shown experimentally in the pioneering work by Andersen.[2] Soon after, Kuriki and Okada demonstrated, based on experimental data, that both ion and electron thermal energy convert preferentially into ion kinetic energy, with the latter conversion due to the development of ambipolar electric fields.[3]

Additional success has been found with self-similar models. These models solve the fluid equations with the assumption that the shape of the radial density profile remains constant throughout the flow. As such,

*Graduate Student, Research Assistant

†Chief Scientist, EPPDyL, Professor, Applied Physics Group, AIAA Fellow

they retain two-dimensional effects in an approximate, contrived way. Recently, Takahasi et al. found good agreement between the experimentally measured thrust of an RF generated plasma expanding through a magnetic nozzle and the thrust predicted from a self-similar model.[4] Their model was later simplified by Fruchtman et al. using the paraxial approximation,[5] which assumes a small magnetic field divergence.

Although quasi one-dimensional and self-similar analytical models have been useful in explaining some of the global expansion properties of magnetic nozzle plasmas, they are limited by their inability to self-consistently capture two-dimensional effects. The nature of magnetic nozzle plasma expansion has been observed both experimentally and with numerical models to exhibit significant spatial non-uniformities. Kuriki and Okada found the plasma potential profile to vary greatly over two-dimensions.[3] Independent experiments by Winglee et al,[6] Deline et al,[7] and Takahashi et al,[8] all observed radial focusing of the plasma density profile with respect to the diverging magnetic field. Numerically solving the two-fluid plasma equations, Ahedo and Merino show a similar focusing resulting from the development of a radial electric field within the downstream plume.[9] Furthermore, they find a strong spatial dependence in the azimuthal current density, electron gyro radius, and Debye length; all important parameters in regards to plasma detachment from the applied magnetic field.[10–12]

I.A. Motivation and Scope

The two-dimensional character of plasma expansion through the divergent portion of a magnetic nozzle was studied in great depth by Ahedo and Merino using numerical simulations.[9] As such, the purpose of this paper is not to repeat their analysis, but to develop from it a novel analytical framework capable of yielding closed-form solutions to describe the spatial dependence of the plasma flow. We will apply this framework to elucidate two phenomena relevant to the application of magnetic nozzle plasmas for space propulsion: (1) radial focusing of the plasma relative to the applied magnetic field and (2) generation of thrust.

Throughout the course of the paper we hope to answer a few fundamental questions, the first of which is concerned with the ability to formulate a tractable analytical solution for both the radial and axial variation of the relevant plasma parameters. Specifically, *is it possible to separate the quasi one-dimensional "mean" behavior of the plasma from its more spatially-dependent "radial" behavior?* To this end, we derive from the collisionless two-fluid plasma equations a two-dimensional separable model capable of yielding closed form analytical solutions for the spatially-dependent plasma density, potential, and ion Mach number.

The idea behind this separable model stemmed from the realization by Ahedo and Merino that the numerical solution to their two-dimensional fluid model, on average, approximated that of the simplified quasi one-dimensional model.[9] As such, we use the results from their numerical model to validate and extend our analytical model.

The application of our model to describe experimentally-observed focusing of the plasma emerging from a magnetic nozzle will also be presented. We aim to answer the following question: *are experimental plasma density measurements consistent with the focusing effect predicted to result from the development of a strong downstream radial electric field?*

Flow reversal of plasma attached to the divergence-less applied magnetic field is a purely two-dimensional effect with strong implications for propulsion performance. Our analytical model allows describing the flow of plasma back towards the plasma source. The natural questions thus arise: *to what extent do two-dimensional effects alter the predicted thrust as compared to quasi one-dimensional models?* and, assuming one has *a priori* knowledge of plasma detachment, *does an optimal detachment location exist at which thrust is maximized?*

After presenting and describing the model in the following section, and demonstrating in Section III how it can be used to obtain closed-form analytical expressions for the spatial variation of the potential, density, and Mach number in the downstream region of a magnetic nozzle plasma, we provide in, Section IV, answers to the questions stated above and conclude with a brief review of the main points of the paper and discuss future applications of the theory, including magnetic nozzle design and plasma detachment analysis.

II. Two-Dimensional Separable Fluid Model

In this section we derive a two-dimensional analytical model for the plasma density, ion Mach number, and electric potential of a collisionless, magnetized plasma flow. The model is focused on describing plasma flow in a magnetic nozzle, but could be extended to any plasma flow along a guide magnetic field that possesses cylindrical symmetry.

II.A. Assumptions and Limitations

We start with a brief discussion of the assumptions and limitations of the model. As stated previously, one goal of this paper is to provide a concise, analytical description of the two-dimensional properties of supersonic, magnetized plasma flow through a magnetic nozzle. To that end, we are compelled to sacrifice physical complexity in lieu of analytical tractability. In the following discussion and throughout the text, however, we will highlight the discarded phenomena and justify its dereliction.

We begin by restricting our analysis to a fully ionized plasma consisting of isothermal electrons and cold ions. This naturally limits the explicit application of the model to highly-ionized plasmas for which the electron temperature is much greater than the ion temperature such as Helicon[13] and ECR plasmas.[14] As such, propulsions concepts that rely on the energization of ions[15,16] are beyond the scope of this model.

Additionally, we make the assumption that the plasma remains collisionless throughout the flow. The influence of collisions on the dynamics of the plasma can be neglected if the characteristic length scale for cross-field diffusion due to Coulomb collisions is much greater than the length scale of the plasma. We showed in a previous paper[17] that this requirement is met in all but the most dense, weakly magnetized magnetic nozzle plasmas.

We should also note that the theory presented here concerns what we regard as the "ideal" flow of plasma along an applied magnetic field. This definition applies to cases where the plasma dynamics can be well-approximated by the conventional compressible flow equations with a single, isothermal electron temperature population. Deviations from this idealization are common and can occur in the form of double layers or quasi-neutral steepening regions.[18,19] The origin of these structures in laboratory plasmas is still under debate, but it seems that their appearance is marked by decreased propulsion performance.[4,19]

The model also employs the common assumptions of quasi neutrality and negligible induced magnetic fields. Quasi neutrality holds as long as the Debye length is much less than the characteristic dimension of the plasma. The induced magnetic field may be safely ignored if the energy density of the magnetic field remains lower than the thermal energy density of the plasma (i.e $\beta < 1$). Both of these requirements are met in a typical laboratory plasma source. In the far downstream region, on the other hand, it is possible that both non-neutral and induced field effects may become dominant, and have been hypothesized to play a pivotal role in plasma detachment.[11,12,20]

The inclusion of plasma detachment in self-consistent theoretical models has proven to be a formidable task. As such, separation of the plasma from the applied magnetic field is beyond the scope of this paper. We will consider this limitation in more detail in Section IV.

II.B. Governing Equations

In light of the above assumptions, the problem is uniquely described by the momentum and continuity equations for the ion and electrons. These eight equations may be cast in the following dimensionless form:

$$\nabla\left(\frac{1}{2}u_i^2+\phi\right)=\mathbf{u}_i\times\left(\frac{\mathbf{B}}{\rho_i}+\nabla\times\mathbf{u}_i\right), \tag{1}$$

$$\nabla\left(\frac{m_e}{2m_i}u_e^2-\phi+\ln n\right)=\mathbf{u}_e\times\left(\frac{\mathbf{B}}{\rho_e}+\nabla\times\frac{m_e\mathbf{u}_e}{m_i}\right), \tag{2}$$

$$\nabla\cdot(n\mathbf{u}_i)=0, \tag{3}$$

$$\nabla\cdot(n\mathbf{u}_e)=0. \tag{4}$$

Here, we have normalized the ion and electron velocities by the ion acoustic velocity, $c_s=(k_bT_e/m_i)^{1/2}$, which is constant throughout the plume for the case of isothermal electrons. The electric potential, Φ, is normalized by the electron temperature, T_e, such that $\phi=e\Phi/kT_e$. Furthermore, $\rho_j=m_jc_s/eB_0L$, represents an *effective* normalized Larmor radius of species j, B_0 the maximum magnetic field, and L the characteristic length scale of the plasma.

II.C. Simplifying Approximations

Using some approximations, we will now reduce Eqs. (1)-(4) to a system of three equations for three unknowns: the ion Mach number, $M = |\mathbf{u}_i - \mathbf{u}_i \cdot \mathbf{e}_\theta|$; the plasma density, n; and the plasma potential, ϕ.

First, we assume the electron mass to be negligible and consider the component of Eq. (2) along the magnetic field unit vector, $\mathbf{b}$, from which we recover the Boltzmann distribution for the electric potential in terms of the plasma density

$$\mathbf{b} \cdot \nabla (\phi - \ln n) = 0. \tag{5}$$

It has been shown under the assumptions outlined in Section II.A that the terms on the right hand side of Eq. (1) do not greatly influence the ion dynamics, even for very small values of ρ_i.[9] Thus, we are free to consider the limit of unmagnetized ions, $\rho_i >> 1$, from which Eq. (1) ultimately yields,

$$\mathbf{s} \cdot \nabla \left(M^2 + 2\phi\right) = 0. \tag{6}$$

Here, $\mathbf{s}$ is the unit vector of the projection of the ion velocity in the $r-z$ plane, $\mathbf{u}_i - \mathbf{u}_i \cdot \mathbf{e}_\theta$. This relationship emphasizes the reliance of the ion motion on the ambipolar electric field as opposed to the magnetic field, which is a valid approximation even for plasmas with magnetized ions. We will eventually expand upon this simplification and include a correction for the magnetic force on the ions.

The final equation comes from integrating Eq. (3) over a control volume, V, bounded by a control surface, S, and applying the divergence theorem,

$$\int_S nM (\mathbf{s} \cdot \mathbf{dA}) = 0. \tag{7}$$

Eqs. (5)-(7) represent an underdetermined system of three equations for four unknowns: M, n, ϕ, $\mathbf{s}$. The only physics eliminated from the governing equations, Eqs. (1)-(4), are electron inertial forces and the magnetic force on ions. We find that it is not necessary to explicitly include the electron force balance perpendicular to the magnetic field as it would introduce the electron azimuthal velocity, $u_{\theta e}$, as another unknown. However, this does not imply we are ignoring the magnetic force on electrons. Rather, this force balance may ultimately be used to determine $u_{\theta e}$ and the azimuthal electron current density, $j_{\theta e}$.

Numerical results from Ahedo and Merino indicate that, even for plasmas where the ion streamlines deviate significantly from their initial magnetic field line, the angle between the two unit vectors remains less than five degrees even far downstream into the plume.[9] Thus, we may close the system of equations by making the additional assumption that the projection of the ion velocity unit vector in the $r-z$ plane, $\mathbf{s}$, is approximately parallel to the magnetic field unit vector, $\mathbf{b}$. We refer to this assumption as *approximately* field-aligned flow.

A subtle yet important distinction must be made at this point between approximately, $\mathbf{s} \approx \mathbf{b}$, and strictly, $\mathbf{s} = \mathbf{b}$, field-aligned plasma flow. In the approximate case, the motion of a given electron is confined to a single magnetic flux surface because of the small electron mass. Ions, however, are able to drift across magnetic flux surfaces as long as quasi neutrality is maintained. Strictly field-aligned plasma flow, on the other hand, is representative of flow in which both ions and electrons are tied to their initial magnetic flux surface. In other words, neither the ions nor electrons are capable of drifting across the magnetic field.

Strictly field-aligned flow inherently assumes highly magnetized ions whose radial expansion is governed primarily by the magnetic force as opposed to ambipolar electric fields. As such, large spatial non-uniformities should not be expected. In fact, the problem becomes drastically simplified because we may rewrite Eq. (7) as $\mathbf{b} \cdot \nabla (nM/B) = 0$, from which the appropriate boundary conditions yield algebraic equations for n, M, and ϕ. Self-similar models,[4,5,7] or those for which the radial density profile is said to scale with the magnetic field, rely on this assumption.

II.D. Coordinate Transformation

With the aim of further simplifying Eqs. (5)-(7), we will now employ a transformation from cylindrical to magnetic coordinates.

The zero divergence property of the magnetic field, $\nabla \cdot \mathbf{B} = 0$, allows us to define a scalar flux function, ψ, which is constant along any magnetic flux surface. Furthermore, neglecting induced currents yields $\nabla \times \mathbf{B} = 0$ and permits the description of $\mathbf{B}$ in terms of a second scaler quantity, ζ, which is constant along any surface

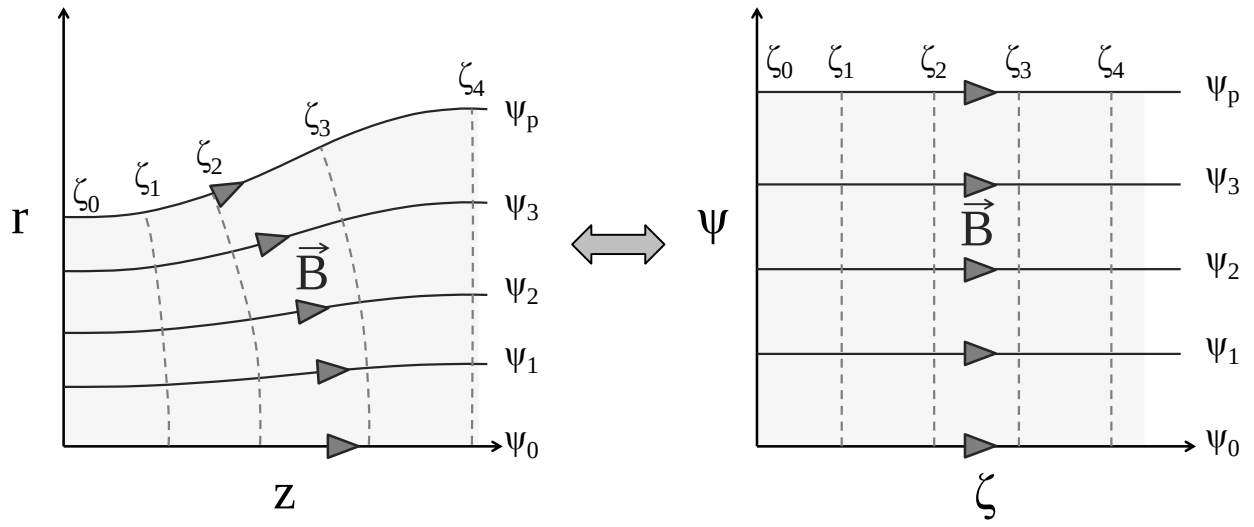

Figure 1. Transformation from cylindrical (r,z) to magnetic (ψ,ζ) coordinates. $\vec{B}$ represents the magnetic field vector aligned along surfaces of constant ψ. The plasma is bounded by ψ_p.

that is everywhere normal to the magnetic field vector. The relationship between the magnetic field and these scalar quantities is given by

$$\mathbf{B} = -\frac{1}{r}\left(\mathbf{e}_\theta \times \nabla\psi\right) = -\nabla\zeta, \tag{8}$$

where $\mathbf{e}_\theta$ is the unit vector in the azimuthal direction. Note that $\nabla\psi \cdot \nabla\zeta = 0$. We will refer to surfaces of constant ψ and ζ as ψ-surfaces and ζ-surfaces, respectively. Figure 1 illustrates the conversion from cylindrical coordinates to magnetic coordinates for a plasma flow contained within the flux surface ψ_p.

Transformation from a cylindrical to magnetic coordinate system, $(r, z) \rightarrow (\psi, \zeta)$, allows the simplification, $\mathbf{b} \cdot \mathbf{dA} = dA$. Here dA is the differential area along a ζ-surface. The integral of a function, $X(\psi, \zeta)$, along a ζ-surface from $\psi \in [0, \psi_p]$ simplifies to

$$\int_\zeta X(\psi,\zeta)dA = 2\pi \int_0^{\psi_p} \frac{X(\psi,\zeta)}{B(\psi,\zeta)} d\psi. \tag{9}$$

Furthermore, the ψ-average of this function is given by

$$\bar{X}(\zeta) = \left[A(\zeta)\right]^{-1} \int_\zeta X(\psi,\zeta)dA, \tag{10}$$

where

$$A(\zeta) = 2\pi \int_0^{\psi_p} \frac{1}{B(\psi,\zeta)} d\psi, \tag{11}$$

is the total area of the ζ-surface.

II.E. Separable Approximation

The coordinate transformation presented in Section II.D enables the separate treatment of the plasma parameters averaged over the beam cross-section and their variation along the beam cross-section. We refer to this approach as the separable approximation.

Specifically, we express the Mach number, plasma potential, and density in the following form:

$$M\left(\psi,\zeta\right) = \bar{M}\left(\zeta\right) + \mathcal{M}\left(\psi,\zeta\right), \tag{12}$$

$$\phi\left(\psi,\zeta\right) = \bar{\phi}\left(\zeta\right) + \varphi\left(\psi,\zeta\right), \tag{13}$$

$$n(\psi,\zeta) = \bar{n}(\zeta) + \mathcal{N}(\psi,\zeta), \tag{14}$$

with the additional requirements

$$\int_\zeta \mathcal{M}(\psi,\zeta)\, dA = 0, \tag{15}$$

$$\int_\zeta \varphi(\psi,\zeta)\, dA = 0, \tag{16}$$

$$\int_\zeta \mathcal{N}(\psi,\zeta)\, dA = 0. \tag{17}$$

Thus, along each ζ-surface the plasma parameters are separated into their ψ-averaged component ($\bar{M}$, $\bar{n}$, $\bar{\phi}$) and a two-dimensional, ψ-dependent correction ($\mathcal{M}$, $\mathcal{N}$, φ), whose average over the entire beam cross-section along the ζ-surface is zero.

II.F. ψ-Averaged Solution

We now assume that there exists a flow plane, defined by $\zeta = \zeta_0$, at which we know the beam-wise variation of the density, $n_0(\psi)$, ion Mach number, $M_0(\psi)$, and potential, $\phi_0(\psi)$. Furthermore, in anticipation of the application of this model to magnetic nozzle plasma flow, we define $M_0(\psi) = 1$ and $\phi_0(\psi) = 0$. However, extension of the model to other boundary conditions is straightforward.

The ζ-evolution of the ψ-averaged plasma parameters may be obtained by averaging Eqs. (5)-(7) over a ζ-surface. This yields,

$$\bar{M}^2 - 1 + 2\bar{\phi} = -\overline{\mathcal{M}^2}, \tag{18}$$

$$\bar{n} - \bar{n}_0 \exp\bar{\phi} = 0, \tag{19}$$

$$\bar{n}\bar{M} - \bar{n}_0\bar{M}_0\frac{A_0}{A} = -\overline{\mathcal{N}\mathcal{M}}, \tag{20}$$

where the quantities on the right-hand side of each equation represent the error due to the separable approximation. In the limit where these errors go to zero, Eqs. (18)-(19) reduce to the known quasi-one-dimensional equations for isothermal, ideal plasma expansion.[2]

II.G. Two-Dimensional Correction

We now turn our attention to the ψ-dependent corrections in Eqs. (12)-(14). The potential correction will be found by considering the force balance on ions in a direction perpendicular to the magnetic field.

As we mentioned earlier, electric fields are the dominant contribution to the ion dynamics. As such, the ion centrifugal force at a given location must be approximately balanced by the electric field. Projecting this force balance onto a ζ-surface gives,

$$rB\frac{d\varphi}{d\psi} = -\frac{M^2}{R_c}. \tag{21}$$

We have introduced here the local radius of curvature of the ion streamline, $R_c = |\mathbf{n}\cdot(\mathbf{s}\cdot\nabla\mathbf{s})|^{-1}$ where $\mathbf{n}$ and $\mathbf{s}$, are the unit vectors perpendicular and parallel to ion streamline, respectively. Note that we do not use the partial derivative in the equation above because we are considering the gradient of φ along a surface of constant ζ. Ultimately, this will allow us to solve for the ψ-dependence of φ along any ζ-surface.

Once again assuming the flow is approximately field-aligned, we express the radius of curvature in terms of the unit vectors perpendicular and parallel to the applied magnetic field, $\mathbf{h}$ and $\mathbf{b}$, respectively: $R_c \approx |\mathbf{h}\cdot(\mathbf{b}\cdot\nabla\mathbf{b})|^{-1}$. This allows R_c to be determined from the applied magnetic field topology.

Substitution of Eq. (6) into Eq. (21) allows the description of the two-dimensional plasma potential correction, φ, in terms of a nonlinear ordinary differential equation in ψ,

$$\frac{d\varphi}{d\psi} + \frac{1 - 2\bar{\phi} - 2\varphi}{rBR_c} = 0. \tag{22}$$

We will show later that this equation is fundamental to the two-dimensional nature of the solution, which indicates the importance of the perpendicular force balance between the electric field and ion dynamic pressure on the global properties of the flow.

We now combine Eqs. (5)-(6) and Eqs. (13)-(14) to find expressions for the ψ-dependent corrections to the ion Mach number and plasma density.

$$\mathcal{M} = -\bar{M} + \left[\bar{M}^2 - 2\varphi\right]^{1/2} \tag{23}$$

$$\mathcal{N} = n_0 \exp\phi - \bar{n} \tag{24}$$

Therefore, we arrive at three equations that may be used to solve for the variation from the mean quantity of each plasma parameter along a ζ-surface.

II.H. Solution Procedure

Our problem is now uniquely defined in terms of six equations for six unknowns. For a given entrance flow and applied magnetic field, Eqs. (18)-(20) may be solved for the mean plasma parameters ($\bar{M}$, $\bar{n}$, $\bar{\phi}$) as a function of ζ.

Eq. (22), subject to the constraint of Eq. (16), provides a two-dimensional expression for φ, which leads, through Eq. (23) and Eq. (24), to expressions for $\mathcal{M}$ and $\mathcal{N}$, respectively.

This represents a fully analytical procedure for finding the two-dimensional Mach number, potential, and density distributions of a collisionless, magnetized plasma flow. We will show in Section III that reasonable approximations allow for closed form solutions for ($\mathcal{M}$, $\mathcal{N}$, φ) in terms of ($\bar{M}$, $\bar{n}$, $\bar{\phi}$). As is well known from compressible flow theory,[1] however, the mathematical nature of Eqs. (18)-(20) yield implicit expressions for ($\bar{M}$, $\bar{n}$, $\bar{\phi}$).

II.I. Inclusion of Ion Magnetization

Although the effective ion Larmor radius, ρ_i, does not significantly change the properties of the flow, it is possible to include a heuristic correction for finite ion magnetization effects in Eq. (21)

$$\frac{d\varphi}{d\psi} + \frac{M^2}{rBR_c}\left(\frac{1 + a\rho_i^{-b}}{1 + a\rho_i^{-b}M^2}\right) = 0. \tag{25}$$

Here, a and b are free parameters. A physical explanation of the form of this equation is provided along with an example in appendix A.

III. Example: Magnetic Nozzle Flow

We will now demonstrate how the two-dimensional separable fluid model for collisionless, magnetized plasma flow can be used to obtain closed-form analytical expressions for the spatial variation of the potential, density, and Mach number in the downstream region of a magnetic nozzle plasma.

III.A. Magnetic Field Model

We begin by defining the coordinate transformation from cylindrical to magnetic coordinates (Figure 2). We assume the applied magnetic field of our nozzle is generated by a single loop of current, from which the ψ-surfaces and ζ-surfaces may be approximated as

$$\psi\left(r, z\right) = \frac{r^2/2}{\left(1 + r^2 + z^2\right)^{3/2}}, \tag{26}$$

$$\zeta\left(r, z\right) = \frac{z/2}{\left(r^2 + z^2\right)^{3/2}}. \tag{27}$$

All lengths above are normalized by the radius of the current loop, r_c. We should note that the equation for ζ given in Eq. (27) is not the exact expression as determined from Eqs. (8) and (26) because it does not exist in closed form. However, we found Eq. (27) to be a valid approximation for values of $z > 1$.

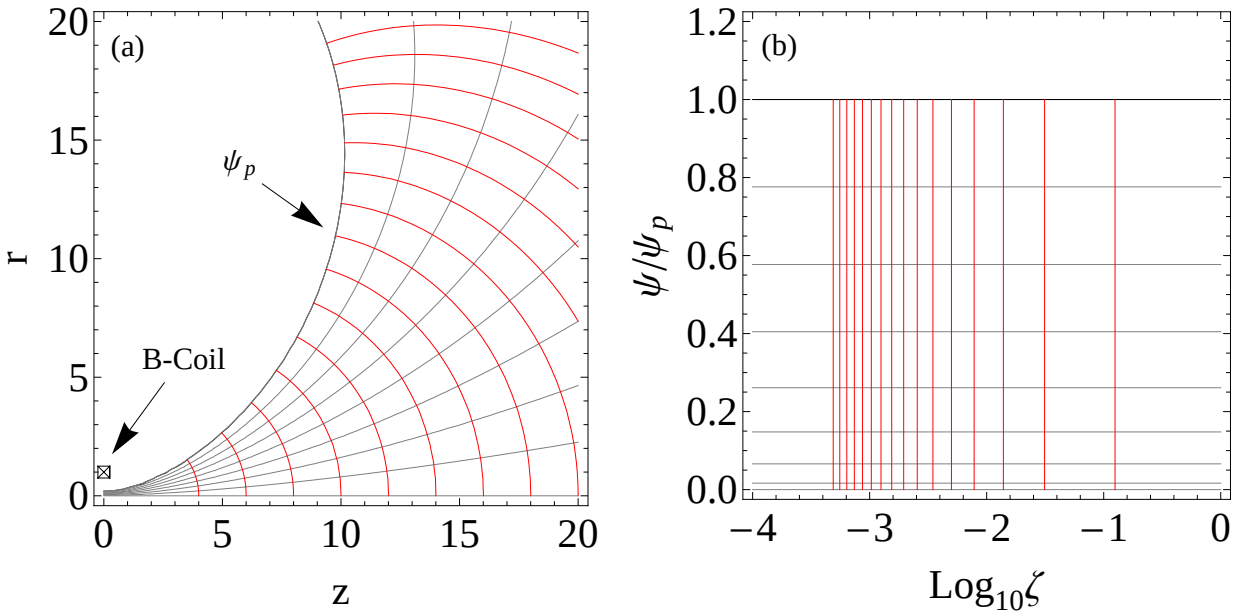

Figure 2. Transformation from cylindrical (r,z) to magnetic (ψ,ζ) coordinates using Eqs. (26)-(27). Distances in (a) are normalized by the radius of the magnetic coil, r_c. Note the flow direction in (a) is for increasing z and in (b) is for decreasing ζ.

III.B. Entrance Conditions

Acceleration of plasma through a magnetic nozzle is similar in many ways to the flow of gas through a conventional de Laval nozzle.[2] As such, a sonic condition forms at the throat of the nozzle, from which we already took $M_0 = 1$. The location of the throat for the above magnetic field occurs at $z = 0$.

An analytical expression for the radial density distribution of plasma confined within a cylindrical vessel was derived by Ahedo.[21] This distribution was used in numerical models by Ahedo and Merino to characterize the two-dimensional expansion of a non-uniform magnetic nozzle plasma.[9] To allow direct comparison with their numerical results, we adopt their expression and transform it to magnetic coordinates as

$$n_0(\psi) = \mathrm{J}_0\left[\sigma a_0 \sqrt{\frac{1-(1-12\psi)^{1/2}}{1-(1-12\psi_p)^{1/2}}}\right]. \tag{28}$$

In this equation, J_0 is the zeroth Bessel function, a_0 is the first zero of J_0, and the factor $\sigma = 0.99$ is used to avoid a singularity at the plasma edge. The expression within the square root is an approximation of the ratio r/r_{p0} at $z = 0$, where r_{p0} is initial the radius of the plasma. This approximation is accurate to within three percent for $r_{p0} < 0.35$. Furthermore, we denote $\psi_p = \psi(r_{p0}, 0)$.

The final entrance condition that we require is the potential distribution at the nozzle throat, ϕ_0. Again, to aid comparison, we follow Ahedo and Merino and set $\phi_0 = 0$.

III.C. Analytical Solution

Armed with a magnetic field model and entrance conditions, our task is now to solve Eqs. (18)-(20) and Eqs.(22)-(24) for ($\bar{M}$, $\bar{n}$, $\bar{\phi}$) and ($\mathcal{M}$, $\mathcal{N}$, φ), respectively.

We assume that the errors due to the separable approximation in Eqs. (18)-(20) are negligible. This is generally satisfied up until the turning point of the applied magnetic field, after which errors in the continuity equation become significant. Substitution of Eq. (26) into Eq. (8) yields an expression for the magnetic field. This expression may then be inserted into Eq. (11) for the cross-sectional area of a given ζ-surface, $A(\zeta)$. This, along with the entrance conditions, permits one to solve Eqs. (18)-(20) for implicit expressions for the ψ-averaged parameters, ($\bar{M}$, $\bar{n}$, $\bar{\phi}$). Considerable simplification of this procedure with minimal error may be achieved with the approximation $A(0)/A(z) \approx B(0,z)/B(0,0)$. This is equivalent to the statement that $B(r,z)$ is constant along a ζ-surface, which is valid for paraxial magnetic fields ($B_r \ll B_z$).

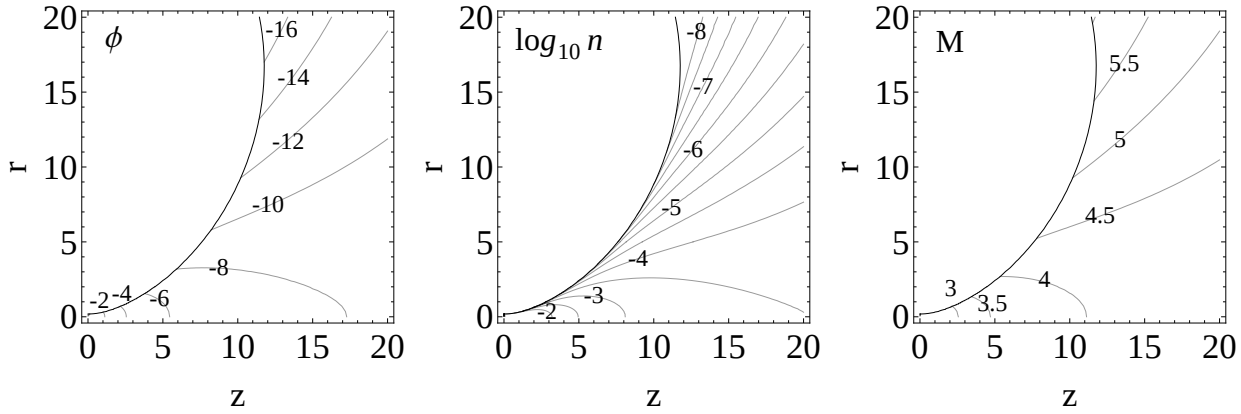

Figure 3. Contour plots of the analytical solution for the potential, ϕ, density, n, and ion Mach number,M, for plasma expansion through a magnetic nozzle. All lengths are normalized by the radius of the magnetic coil, r_c. Solutions are found using Eqs. (23),(24) and (32) for an initial plasma radius $r_{p0} = 0.185$.

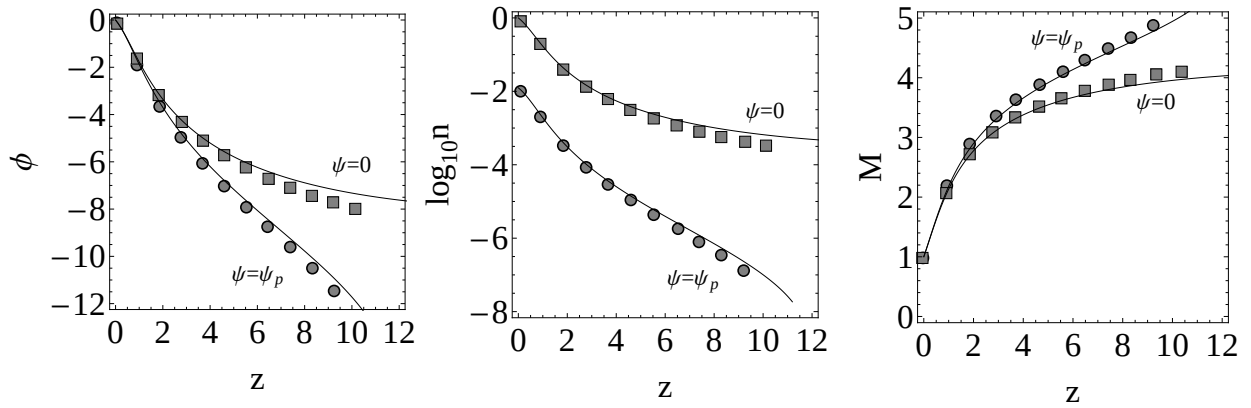

Figure 4. Comparison of the analytical solution (solid line) for the potential, ϕ, density, n, and ion Mach number,M to the numerical results (shaded points) shown in Fig. 4 of Ref. [9]. Note that the x-axis of the numerical data was adjusted to be consistent with our normalization.

We now turn our attention to Eq. (22) to find an expression for φ. An analytical solution to this equation in its present form is not possible due to the complexity of the denominator of the second term, rBR_c. To make the equation more tractable, we define $K \equiv (rBR_c)^{-1}$, and take the Taylor series of K about $\psi = 0$. The result gives

$$K(\psi, \zeta) \approx f_1(\zeta) + \psi f_2(\zeta), \tag{29}$$

where the functions

$$f_1(\zeta) = \frac{3\sqrt{2}}{8}\left[\frac{1+4\zeta}{\sqrt{\zeta(1+2\zeta)}}\right] \approx \frac{3}{4\sqrt{2}}\zeta^{-1/2}, \tag{30}$$

$$f_2(\zeta) = \frac{3}{16}\left[\frac{3+16\zeta+56\zeta^2}{\zeta(1+2\zeta)}\right] \approx \frac{9}{16}\zeta^{-1}, \tag{31}$$

are found by averaging the zeroth and first-order Taylor series expansions. The approximations on the right hand side of Eqs. (30) and (31) are valid in the limit $\zeta < 1$ (equivalent to $z > 1$). Furthermore, by analyzing the error due to the approximation for different values of ζ and ψ, we found that Eq. (29) yields reasonable accuracy in the range: $\zeta \in [10^{-4}, 1]$ and $r_{p0} \in [0, 0.35]$.

Substitution of Eq. (29) into the first-order differential equation for φ, Eq. (22), yields an analytical expression for φ. The integration constant may be found from Eq. (16). The result, combined with Eq. (13), yields

$$\phi(\psi, \zeta) = \frac{1}{2} - \frac{f_\phi(\zeta)}{\sqrt{\pi}} \exp\left[\frac{1}{16\zeta}\left(2\sqrt{2\zeta} + 3\psi\right)^2\right], \tag{32}$$

with

$$f_\phi(\zeta) = \frac{3\psi_p}{4\sqrt{\zeta}} \left[\frac{\bar{\phi}(\zeta) - 1}{\text{Erfi}\left(1/\sqrt{2}\right) - \text{Erfi}\left(1/\sqrt{2} + 3\psi_p/4\sqrt{\zeta}\right)} \right]. \tag{33}$$

Eqs. (32) and (33) represent a closed form analytical solution for the plasma potential in terms of the two-dimensional magnetic coordinate system. Conversion back to cylindrical coordinates may be achieved using Eqs. (26) and (27).

Finally, closed formed solutions for the ion Mach number and plasma density may be obtained from substitution of Eq. (32) into Eqs.(23) and (24). We omit here the explicit form of these equations for the sake of brevity.

Contour plots demonstrating the clear two-dimensional behavior of the plasma potential, density, and ion Mach number are presented in Figure 3. The initial plasma radius is taken to be $r_{p0} = 0.185$. A number of observations may be made about the nature of this flow:

- A large potential well develops along the plasma edge in the far field of the plume. This is due to the increased magnetic field curvature in this region, which causes ion inertia and the tendency of the plasma to remain quasi-neutral to lead to a large potential gradient in the direction perpendicular to the magnetic field.
- The increased potential gradient near the edge of the plume leads to a rarefaction of the plasma edge as fewer electrons are capable of entering the potential well. Depending on the initial plasma density, plasma quasi-neutrality may ultimately be violated in this region.
- Rarefaction at the plasma edge leads to the relative focusing of the beam profile with respect to the expanding magnetic field.
- Ion acceleration occurs near the nozzle axis in the initial expansion region but is impeded in the far field region. This is in contrast to the edge of the plasma, whereby ion acceleration continues throughout the far-field.

These observations are in qualitative agreement with the analysis of Ahedo and Merino based on their numerical solution to the same problem.[9] Furthermore, they allow an extension of their results to the region beyond the turning point of the plasma boundary ($z \approx 11$ in Figure 3).

III.D. Comparison to Numerical Results

We now proceed to a more quantitative comparison of the two-dimensional separable solution to the numerical results of Ahedo and Merino.[9] Specifically, we take sample points from Figure 4 in Ref.[9] to compare the analytical and numerical solutions for the axial dependence of the potential, density, and Mach number along both the nozzle axis, $\psi = 0$, and plasma edge, $\psi = \psi_p$. This comparison is shown in Figure 4.

A quick note on the origin of Figure 4: of the three curves with varying ρ_i shown in Figure 4 of Ref.[9], we choose sample points from the curve for $\rho_i = 10$. As such, the analytical expressions in Fig. 4. do not include the ion magnetization correction described in Section II.I.

A strikingly good agreement is found between the analytical solution to the two-dimensional separable equations and the numerical solution to the full two-fluid equations. Specifically, the analytical solution accurately tracks the non-uniformity in the plasma potential and Mach number that develops in the downstream region. Furthermore, the increased rarefaction of the plasma along its boundary as predicted by the analytical solution matches that of the numerical solution. Deviations of the predicted potential from the numerical solution occur in the far field of the plume, but are limited to just a few percent. This discrepancy is likely due to the magnetic field approximation.

IV. Applications

We present in this section two applications of the two-dimensional analytical model for magnetic nozzle plasma expansion: (1) an explanation of experimentally observed plasma focusing, and (2) a preliminary analysis of the implications of two-dimensional effects on propulsion performance.

IV.A. Plasma Focusing in Magnetic Nozzle Experiments

Interest in plasma detachment from magnetic nozzles has provided multiple experimental studies of the axial evolution of the radial density profile in magnetic nozzle plasma plumes.[3,6–8] Many of these studies have observed focusing of the plasma beam with respect to the expanding magnetic field lines.[6–8]

A variety of explanations for this phenomenon have been put forth. Deline showed that the location where focusing becomes noticeable in his experiment corresponds to the point in the flow where the plasma kinetic energy density exceeds the applied field energy density.[7] This led him to suggest, in accordance with the MHD plasma detachment scenario of Arefiev and Breizman,[11] that the focusing is due to the effective detachment of both the ions and electrons from the applied magnetic field. Takahashi et al.,[8] on the other hand, concluded that the focusing effect observed in their experiment results from separation of only the ions from the magnetic field.

We are now prepared to answer the question that we posed at the outset: *are experimental plasma density measurements consistent with the focusing effect predicted to result from the development of a strong downstream radial electric field?*

We begin by fitting our analytical model to data from three independent experiments: (1) Deline et. al.[7] used Langmuir and Faraday probes to measure both the half-width at half-maximum (HWHM) of the radial density profile (Figure 5(a)) and the on-axis ion current (Figure 5(b)) of a coaxial gun plasma expanding through the magnetic field of electromagnetic coils; (2) Takahashi et. al.[8] used a retarding field energy analyzer (RFEA) to determine the HWHM of the radial density profile (Figure 5(c)) for the expansion through permanent magnetics of an inductively-coupled, RF plasma; and, in a later experiment, (3) Takahashi et. al.[4] measured the on-axis plasma density (Figure 5(d)) using a Langmuir probe in an RF (mode unspecified) plasma flow through a single electromagnetic coil (Case B in Ref.[4]).

A number of steps were required to allow the data to be analyzed within the context of the normalized coordinate system of the analytical model. These steps are as follows:

1. The lengths provided in the referred publications are normalized using the effective plasma coil radius. This is found by fitting the equation, $B(z) = B_0 \left(1 + (z/r_c)^2\right)^{-3/2}$, to the reported measurements of the on-axis magnetic field strength for each experiment. Here, B_0 is the value of the maximum magnetic field strength. This procedure yields $r_{c,1} = 15$ cm, $r_{c,2} = 8.5$ cm, and $r_{c,3} = 9$ cm for experiments 1-3, respectively. We note that these values approximate that of the physical radius of the electromagnetic coil/permanent magnet for each experiment.

2. The analytical curve in Figure 5(a) is found using the density profile of Eq. (28) and adjusting the initial plasma radius such that the curve approximately passes through the data point at $z \approx 3$. This resulted in $r_{p0} = 0.167$.

3. The data in Figure 5(b) is normalized to match the data point at $z \approx 3$ to the analytical curve. The entrance conditions used to obtain this curve are the same as those used in Figure 5(a).

4. The analytical curve in Figure 5(c) is obtained by setting the initial radius equal to the diameter of the plasma source used in the experiment, $r_{p0} = 0.388$. We used the entrance density profile provided in Ref.[4] for the same plasma source.

5. The initial radius for the analytical curve in Figure 5(d) is found by approximately fitting the analytical curve to the first few data points. This procedure gives $r_{p0} = 0.39$, which is less than the radius of the plasma source, $r_s = 0.5$. This is justified, however, because the retraction of the magnetic coil from the exit of the plasma source should produce an effective plasma radius less than that of the source (see Figure 2(b) in Ref.[4]). The radial density profile is also obtained from Ref.[4].

The normalized experimental data from these experiments is presented in Figures 5(a)-(d) along with analytical curves found using the two-dimensional separable solution presented in Section III. Also shown is the scaling associated with plasma flow for which both the ions and electrons remain attached to the magnetic field.

The experimental data show two clear trends that result from focusing of the plasma beam with respect to the diverging magnetic field: (1) the HWHM deviates significantly from its initial ψ-surface towards the nozzle axis, and (2) the on-axis ion flux, J_i, and density, n, are much greater than the values predicted from the magnetic field scaling (i.e. the self-similar model).

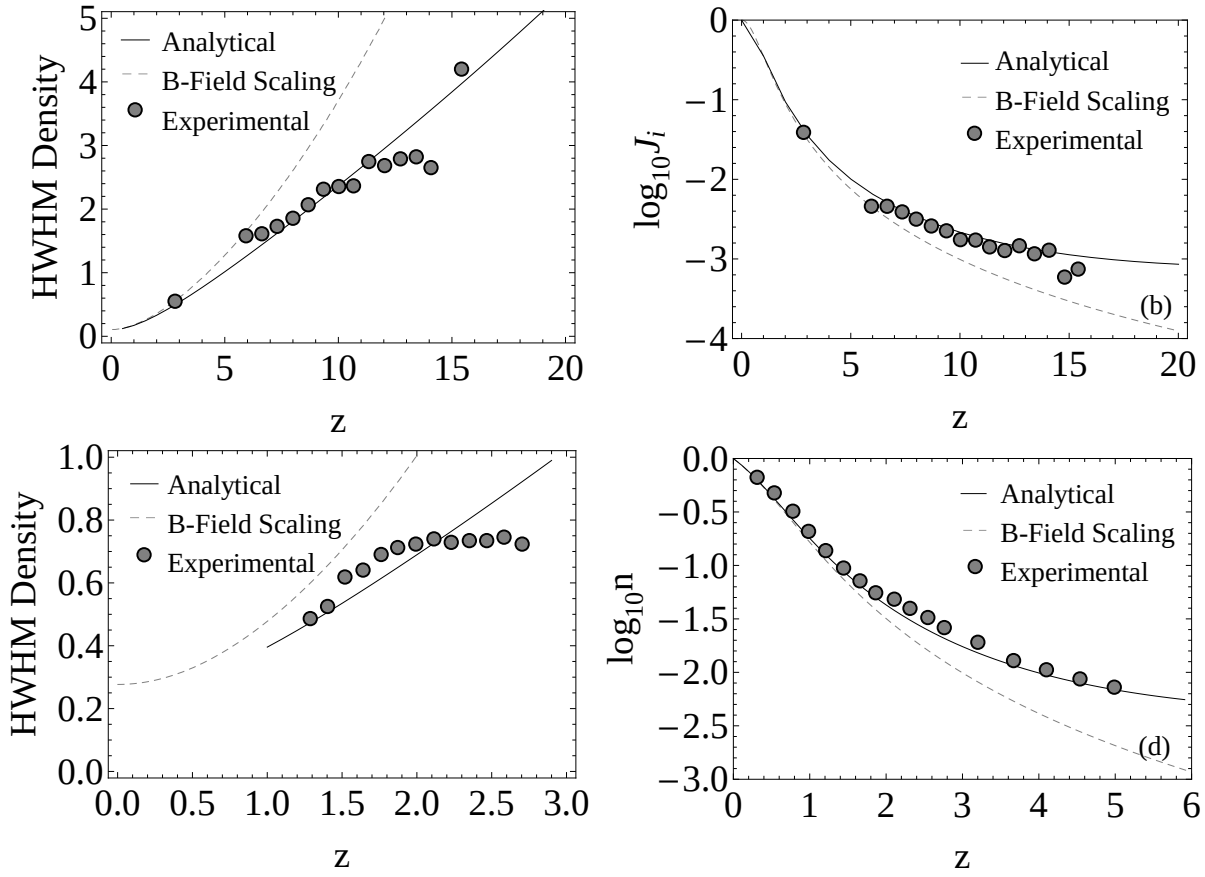

.

Figure 5. Application of the separable analytical model (solid lines) to experimental results (shaded points) for: (a) HWHM of the radial density profile along the nozzle axis from Ref. [7]; (b) on-axis ion flux, J_i, from Ref.[7]; (c) HWHM of the radial density profile along the nozzle axis from Ref.[8]; and (d) on-axis density, n, from Ref.[4]. The dashed lines show the expected scaling for uniformly magnetized plasma flow.

It is clear from Figure (6) that the two-dimensional correction to the quasi one-dimensional equations described in Section II accurately reproduces both of the trends that result from plasma focusing. This indicates to us that the experimentally observed focusing of the plasma with respect to the applied magnetic field is, in accordance with the analysis of Ahedo and Merino,[9] due to the formation of radial electric fields that manifest from the ion kinetic pressure and the preservation of quasi neutrality. This picture is consistent with the explanation by Takahasi[8] that the deviation of the HWHM occurs due to ion separation. As a consequence, deviation of the density profile HWHM from its initial flux surface indicates the onset of ion cross-field drift, but not necessarily plasma detachment.

IV.B. Implications for Nozzle Performance

The ability to characterize the plasma flow of a magnetic nozzle beyond the turning point of the applied magnetic field gives our model the unique ability to investigate the trade-off between the momentum gain from further expansion and the divergence of the flow and its influence on the predicted thrust. If the plasma is unable to detach from the applied magnetic field, the flow divergence will negate the momentum gain.

We define the thrust coefficient of the nozzle as the ratio of the ψ-averaged axial momentum flux of the plasma flow through a ζ-surface to the mean pressure force at the nozzle throat,

$$C_T \equiv \frac{F_z}{\bar{p}_0 A_0} = \int_\zeta \left(M^2+1\right) \frac{B_z}{B} \frac{ndA}{n_0 A_0}. \tag{34}$$

Here, we have again considered the flow to be approximately field-aligned, $\mathbf{s} \approx \mathbf{b}$. We note that the thrust coefficient given in Eq. (34) is a function of ζ. Under the questionable assumption that the plasma detaches

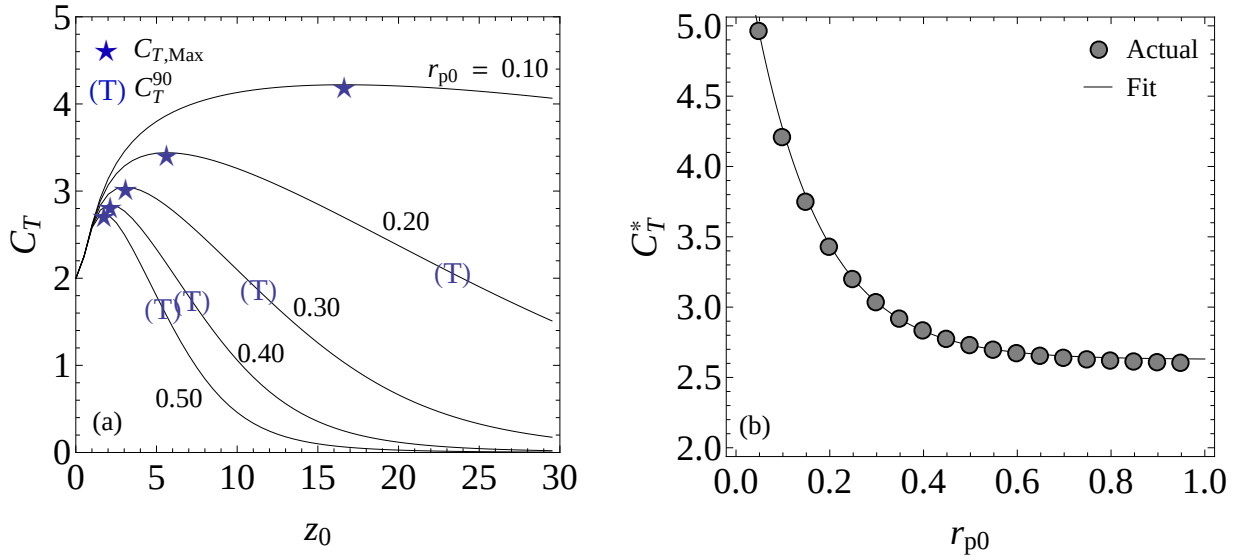

Figure 6. (a) Variation of the thrust coefficient throughout the plume shows clear locations for maximum thrust marked by stars. Curves are shown for $r_{p0} \in [0, 0.5]$. $z_0(\zeta)$ is the axial location at which the ζ-surface intersects the nozzle axis. (b) Value of the maximum thrust coefficient versus the initial plasma radius.

from the applied field, and that momentum transfer is not transfered beyond a surface defined by $\zeta = \zeta_{det}$, the thrust coefficient may be determined from $C_T(\zeta_{det})$.

Immediately, we see from Eq. (34) that a competition will occur as expansion of the plasma increases $n(M^2 + 1)$ but decreases the ratio B_z/B. We may approximate this ratio as

$$\frac{B_z}{B} \approx 1 - 2\frac{\psi}{\psi_p}\sin^2\left(\frac{\alpha_p}{2}\right), \tag{35}$$

where α_p is the angle that the magnetic field vector makes with the nozzle axis along the plasma boundary, $\psi = \psi_p$. Note that α_p is a function of only ζ.

We admit at this point the main fallacy of the theoretical model presented in Section II: strict conservation of mass and momentum is valid only in the limit where the errors on the right hand side of Eqs. (18)-(20) are vanishingly small. This is not ensured by the two-dimensional separable model in its current form. As such, we cannot quantify the influence of plasma focusing on the thrust coefficient. Conservation of the mass and momentum is valid for the mean parameters, however, and we abandon the ψ-dependent corrections ($\mathcal{M}$, $\mathcal{N}$, φ) in the following discussion.

Substitution of Eq. (35) into Eq. (34) yields a simplified form for the thrust coefficient,

$$C_T = \frac{\bar{n}A\left(\bar{M}^2 + 1\right)}{\bar{n}_0 A_0}\cos^2\left(\frac{\alpha_p}{2}\right) \tag{36}$$

This expression is plotted in Figure 6(a) for five values of $r_{p0} \in [0, 0.5]$. We note that the horizontal axis corresponds to the axial distance at which the ζ-surface intersects $r = 0$, or $z_0 = (2\zeta)^{-1/2}$.

A clear maximum is demonstrated for the thrust coefficient in Figure 6(a). The values of these maxima, C_T^*, are marked with stars. We also indicate the value, C_T^{90}, that corresponds to the ζ-surface for which the edge of the plume has turned a full ninety degrees, or $\alpha_p = \pi/2$. Of course, it is beneficial to prevent expansion of the plasma beyond the turning point of the applied magnetic field.

It is interesting to note that the thrust measurements taken by Takahashi et al.[4] were obtained for plasmas whose bounding flux surface intersect the walls of their vacuum chamber near the location of C_T^{90}. The measured thrust would indicate a value of $C_T \approx 2$, in accordance with the predictions of Figure 6(a). Two conclusions relevant to their experiment may then be made: (1) an efficiency increase of $\left(C_T^*/C_T^{90}\right)^2 \sim 2$ is possible if they find a way to force plasma detachment closer to the nozzle, and (2) a significant decrease in performance could be expected if the thruster were to operate in a larger vacuum chamber.

Finally, we estimate the maximum thrust for a given plasma source by plotting the maximum thrust coefficient, $C_{T,max}$, versus the normalized plasma radius, $r_{p,0}$. This is shown in Figure 6(b). The data is

well represented by the equation

$$C_T^* \approx c_1 e^{-c_2(r_p/r_c)} + c_3, \tag{37}$$

where $c_1 = 3.28$, $c_2 = 6.97$, and $c_3 = 2.63$ result from the method of least-squares.

V. Conclusions

An analytical model was derived that is capable of reproducing the two-dimensional profile of the potential, density, and ion Mach number of an axisymmetric plasma flow along magnetic field lines. Application of this model to magnetic nozzle plasmas allows us to draw the following conclusions:

- Experimentally observed focusing of the plasma exhaust of a magnetic nozzle with respect to its applied magnetic field can be explained analytically in terms of the development of a radial electric field in the downstream region. As such, this phenomenon does not necessarily preclude detachment of the plasma from its guiding magnetic field.
- The competition in the expansion process between the conversion of thermal energy into kinetic energy and the loss of useful kinetic energy to plume divergence leads to an optimum detachment location at which thrust is maximized.

The main limitations of the analytical model, which prevent its use in a detailed magnetic nozzle thrust model, are its non-conservation of mass and momentum and its inability to self-consistently incorporate physical processes relevant to plasma detachment, such as induced magnetic fields and non-neutral effects. These limitations will be the topic of future research.

Appendix A: Ion Magnetization

In Section II.G. we used an approximate equation for the ion force balance perpendicular to its streamline, Eq. (22), to find the ψ-dependent potential correction, φ, for the case of unmagnetized ions, $\rho_i >> 1$. A correction to that equation that includes finite ion magnetization effects was presented in Section II.I, Eq.(25). In this appendix, we will describe the physical reasoning in going from Eq. (22) to Eq. (25).

Eq. (22) was derived assuming the ion dynamics are influenced only by the ambipolar electric fields that result from the desire of the plasma to remain quasineutral. In reality, there will also be a Lorentz force on the ions due to their motion perpendicular to the applied magnetic field. The azimuthal ion velocity, induced to conserve canonical angular momentum due to ion cross-field motion, leads to a restoring force that tries to push the ions back onto their initial flux surface. Thus, the appropriate form of Eq. (22)) to account for the magnetic force may be written as:

$$\frac{M^2}{R_c} + rB\frac{\partial \varphi}{\partial \psi} - \frac{u_{\theta_i} B}{\rho_i} = 0. \tag{38}$$

The first, second, and third terms on the left hand side are the ion centrifugal force, the force due to the ambipolar electric field, and the magnetic force, respectively. Furthermore, the normalizations are in accordance with those presented in Section II.

Our task now becomes to find an expression for the azimuthal ion velocity in terms of the parameters of our model. Taking the dot product of Eq. (1) with the direction normal to the ion velocity, $\mathbf{n}$, and applying the conservation of ion energy and canonical angular momentum yields

$$u_{\theta,i}/\rho_i = \omega_{\theta,i} e^{-\phi}, \tag{39}$$

where $\omega_{\theta,i}$ is the azimuthal component of the ion vorticity, $\boldsymbol{\omega} = \boldsymbol{\nabla} \times \mathbf{u}$. This equation carries the additional assumption that the initial ion azimuthal velocity and potential are both zero.

We now consider the limit that the ions are highly magnetized, $\rho_i << 1$, and remain attached to their initial magnetic flux surface. Eventually we will arrive at a heuristic solution that is combination of the unmagnetized and highly magnetized results.

For the highly magnetized case, the ion velocity vector is parallel with the magnetic field vector, $\mathbf{s} = \mathbf{b}$, and we may adopt the following simplification for the azimuthal ion vorticity,

$$\omega_{\theta,i} = \theta \cdot (\nabla \times \mathbf{u}) \approx B\left[\mathbf{n} \cdot \nabla\left(\frac{u}{B}\right)\right]. \tag{40}$$

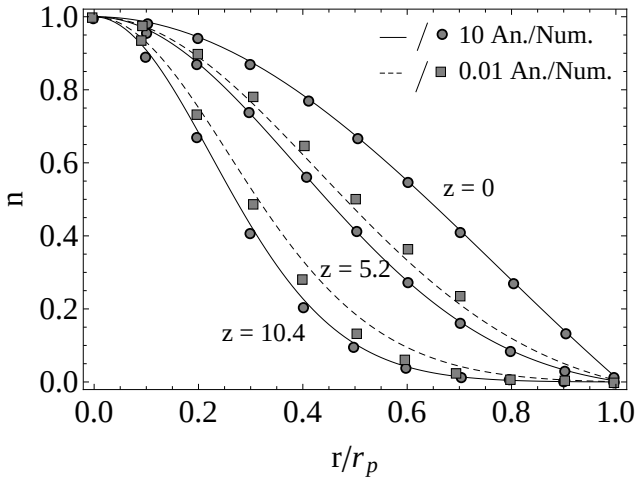

Figure 7. Comparison of the radial density profile for $\rho_i = 10$ and $\rho_i = 0.01$ using Eq. (43) and the numerical results from Ref. [9]. Values of $a = 0.02$ and $b = 1/3$ are used in Eq. (43).

Furthermore, the ion continuity equation ensures that

$$\mathbf{u} \cdot \nabla \left(\frac{nu}{B} \right) = 0. \tag{41}$$

Finally, we may combine Eq. (5) with Eqs. (39)-(41) to arrive at an expression for the azimuthal ion velocity in terms of the effective ion Larmor radius, ρ_i, radial coordinate, r, ion Mach number, M, and the derivative of the two-dimensional potential correction, φ, with respect to ψ,

$$u_{\theta,i}/\rho_i \approx -rM^2 \frac{\partial \varphi}{\partial \psi}. \tag{42}$$

The equation above is valid for entrance flows that satisfy $M_0 = 1$.

A new expression for the ψ-dependent potential correction, valid for highly magnetized ions, results from substitution of Eq. (42) into Eq. (38). We summarize this result along with Eq. (21) as

$$\frac{\partial \varphi}{\partial \psi} = \begin{cases} KM^2 & \text{for } \rho_i \gg 1 \\ KM^2 \left(1 + M^2\right)^{-1} & \text{for } \rho_i \ll 1 \end{cases}$$

where $K = (rBR_c)^{-1}$. In the unmagnetized case, $\rho_i \gg 1$, the potential gradient increases with the square of the Mach number because the electric field in the normal direction must balance the ion dynamic pressure. For the case where the ions are highly magnetized, $\rho_i \ll 1$, ion confinement is helped by the Lorentz force on the ions, for which the potential gradient is allowed to decrease by the factor $(1 + M^2)$.

Possessing knowledge of the projection of the potential gradient along a ζ-surface for both unmagnetized and highly magnetized ions, we now propose the following heuristic equation for the influence of the effective ion Larmor radius on the two-dimensional flow properties:

$$\frac{d\varphi}{d\psi} + KM^2 \left(\frac{1 + a\rho_i^{-b}}{1 + a\rho_i^{-b} M^2} \right) = 0. \tag{43}$$

Here, a and b are empirically determined constants.

Application of the ion magnetization correction to the magnetic nozzle example in Section IV gives values of $a \approx 0.02$ and $b \approx 1/3$. These numbers were obtained by comparing the radial density profile at two different downstream locations with the numerical results of Ahedo and Merino for values of $\rho_i = 0.01$ and $\rho_i = 10$. This comparison is shown in Figure 7. Additional numerical and experimental results are required to further validate Eq. (43). However, as we mentioned is Section IV, this correction is only necessary for highly magnetized flows for which $\rho_i \ll 1$.

Acknowledgments

This work is supported by the Air Force Office of Scientific Research through the National Defense Science and Engineering Graduate Fellowship. Further support comes from the Program in Plasma Science and Technology at the Princeton Plasma Physics Laboratory. The authors would like to thank Professor Eduardo Ahedo and Mario Merino for insightful discussions related to plasma detachment.

References

[1]Hill, P. G. and Peterson, C. R., Mechanics and thermodynamics of propulsion (2nd revised and enlarged edition), 1992.

[2]Andersen, S., Jensen, V., Nielsen, P., and D'Angelo, N., "Continuous supersonic plasma wind tunnel," Physics Letters A, Vol. 27, No. 8, 1968, pp. 527–528.

[3]Kuriki, K. and Okada, O., "Experimental Study of a Plasma Flow in a Magnetic Nozzle," Physics of Fluids, Vol. 13, 1970, pp. 2262.

[4]Takahashi, K., Lafleur, T., Charles, C., Alexander, P., and Boswell, R., "Electron Diamagnetic Effect on Axial Force in an Expanding Plasma: Experiments and Theory," Physical Review Letters, Vol. 107, No. 23, Nov. 2011, pp. 1–4.

[5]Fruchtman, a., Takahashi, K., Charles, C., and Boswell, R. W., "A magnetic nozzle calculation of the force on a plasma," Physics of Plasmas, Vol. 19, No. 3, 2012, pp. 033507.

[6]Winglee, R., Ziemba, T., Giersch, L., Prager, J., Carscadden, J., and Roberson, B. R., "Simulation and laboratory validation of magnetic nozzle effects for the high power helicon thruster," Physics of Plasmas, Vol. 14, No. 6, 2007, pp. 063501.

[7]Deline, C. a., Bengtson, R. D., Breizman, B. N., Tushentsov, M. R., Jones, J. E., Chavers, D. G., Dobson, C. C., and Schuettpelz, B. M., "Plume detachment from a magnetic nozzle," Physics of Plasmas, Vol. 16, No. 3, 2009, pp. 033502.

[8]Takahashi, K., Itoh, Y., and Fujiwara, T., "Operation of a permanent-magnets- expanding plasma source connected to a large-volume diffusion chamber," Journal of Physics D: Applied Physics, Vol. 44, No. 1, Jan. 2011, pp. 015204.

[9]Ahedo, E. and Merino, M., "Two-dimensional supersonic plasma acceleration in a magnetic nozzle," Physics of Plasmas, Vol. 17, No. 1, 2010, pp. 1–16.

[10]Hooper, E., "Plasma detachment from a magnetic nozzle," Journal of Propulsion and Power, Vol. 9, No. 5, 1993, pp. 757–763.

[11]Arefiev, A. V. and Breizman, B. N., "Magnetohydrodynamic scenario of plasma detachment in a magnetic nozzle," Physics of Plasmas, Vol. 12, No. 4, 2005, pp. 043504.

[12]Ahedo, E. and Merino, M., "On plasma detachment in propulsive magnetic nozzles," Physics of Plasmas, Vol. 18, No. 5, 2011, pp. 053504.

[13]Batishchev, O. V., "Minihelicon Plasma Thruster," IEEE Transactions on Plasma Science, Vol. 37, No. 8, Aug. 2009, pp. 1563–1571.

[14]Popov, O. a., "Characteristics of electron cyclotron resonance plasma sources," Journal of Vacuum Science & Technology A: Vacuum, Surfaces, and Films, Vol. 7, No. 3, May 1989, pp. 894.

[15]Bering, E., Changdiaz, F., Squire, J., Brukardt, M., Glover, T., Bengtson, R., Jacobson, V., Mccaskill, G., and Cassady, L., "Electromagnetic ion cyclotron resonance heating in the VASIMR," Advances in Space Research, Vol. 42, No. 1, July 2008, pp. 192–205.

[16]Jorns, B. and Choueiri, E., "Ion Heating with Beating Electrostatic Waves," Physical Review Letters, Vol. 106, No. 8, Feb. 2011, pp. 2–5.

[17]Little, J. M., Rubin, A. S., and Choueiri, E. Y., "Similarity Parameter Evolution within a Magnetic Nozzle with Applications to Laboratory Plasmas," 32nd International Electric Propulsion Conference, 2011, pp. 1–24.

[18]Charles, C. and Boswell, R., "Current-free double-layer formation in a high-density helicon discharge," Applied Physics Letters, Vol. 82, No. 9, 2003, pp. 1356.

[19]Ahedo, E., "Double-layer formation and propulsive assessment for a three-species plasma expanding in a magnetic nozzle," Physics of Plasmas, Vol. 18, No. 3, 2011, pp. 033510.

[20]Roberson, B. R., Winglee, R., and Prager, J., "Enhanced diamagnetic perturbations and electric currents observed downstream of the high power helicon," Physics of Plasmas, Vol. 18, No. 5, 2011, pp. 053505.

[21]Ahedo, E., "Parametric analysis of a magnetized cylindrical plasma," Physics of Plasmas, Vol. 16, No. 11, 2009, pp. 113503.